



Article

Multifunctional Graphene-Polymer Nanocomposite Sensors Formed by One-Step In Situ Shear Exfoliation of Graphite

Ali Ashraf ^{1,*} ⁰, Elizabeth Chang ², Md Ashiqur Rahman ¹ ⁰, Dipannita Ghosh ³, Nazmul Islam ³ and Jennifer K. Lynch-Branzoi ^{2,*} ⁰

- Department of Mechanical Engineering, University of Texas Rio Grande Valley, Edinburg, TX 78539, USA; mdashiqur.rahman01@utrgv.edu
- Mechanical and Aerospace Engineering Department, Rutgers University, New Brunswick, NJ 08854, USA; lizchang718@gmail.com
- Department of Electrical & Computer Engineering, University of Texas Rio Grande Valley, Edinburg, TX 78539, USA; dipannita.ghosh01@utrgv.edu (D.G.); nazmul.islam@utrgv.edu (N.I.)
- * Correspondence: ali.ashraf@utrgv.edu (A.A.); jklynch@soe.rutgers.edu (J.K.L.-B.)

Abstract: Graphene nanocomposites are a promising class of advanced materials for sensing applications; yet, their commercialization is hindered due to impurity incorporation during fabrication and high costs. The aim of this work is to prepare graphene-polysulfone (G-PSU) and graphenepolyvinylidene fluoride (G-PVDF) nanocomposites that perform as multifunctional sensors and are formed using a one-step, in situ exfoliation process whereby graphite is exfoliated into graphene nanoflakes (GNFs) directly within the polymer. This low-cost method creates a nanocomposite while avoiding impurity exposure since the raw materials used in the in situ shear exfoliation process are graphite and polymers. The morphology, structure, thermal properties, and flexural properties were determined for G-PSU and G-PVDF nanocomposites, as well as the electromechanical sensor capability during cyclic flexural loading, temperature sensor testing while heating and cooling, and electrochemical sensor capability to detect dopamine while sensing data wirelessly. G-PSU and G-PVDF nanocomposites show superior mechanical characteristics (gauge factor around 27 and significantly enhanced modulus), thermal characteristics (stability up to 500 °C and 170 °C for G-PSU and G-PVDF, respectively), electrical characteristics (0.1 S/m and 1 S/m conductivity for G-PSU and G-PVDF, respectively), and distinguished resonant peaks for wireless sensing (~212 MHz and ~429 MHz). These uniquely formed G-PMC nanocomposites are promising candidates as strain sensors for structural health monitoring, as temperature sensors for use in automobiles and aerospace applications, and as electrochemical sensors for health care and disease diagnostics.

Keywords: graphene; polymer; nanocomposite; sensing



Citation: Ashraf, A.; Chang, E.; Rahman, M.A.; Ghosh, D.; Islam, N.; Lynch-Branzoi, J.K. Multifunctional Graphene–Polymer Nanocomposite Sensors Formed by One-Step In Situ Shear Exfoliation of Graphite. *J.* Compos. Sci. 2023, 7, 309. https:// doi.org/10.3390/jcs7080309

Academic Editor: Francesco Tornabene

Received: 16 June 2023 Revised: 19 July 2023 Accepted: 24 July 2023 Published: 27 July 2023



Copyright: © 2023 by the authors. Licensee MDPI, Basel, Switzerland. This article is an open access article distributed under the terms and conditions of the Creative Commons Attribution (CC BY) license (https://creativecommons.org/licenses/by/4.0/).

1. Introduction

Multifunctional flexible sensors are gaining more and more importance these days due to applications in the automotive, aerospace, bio, and structural health, marine, and energy sectors [1–4]. Strain sensors can be made from different materials like metals and polymers with different fillers. Polymers are intrinsically poor in electrical and thermal conductivity and require conductive fillers to enhance those properties for sensing applications. Among different conductive fillers, graphene (single, few, and multi-layer) and exfoliated graphite are of great interest due to their exceptional mechanical properties [5], thermal and electrical conductivities, stability, and large surface area [6,7]. This class of graphene-enhanced thermoplastic polymer matrix composite, henceforth referred to as G–PMC, depends on the unique properties of both graphene/graphite and the polymer to sense its environment. Graphene materials (graphene, graphene oxide, graphene composites) with varying properties can be synthesized by electrochemical exfoliation [8]. Khakpour et al. exfoliated a graphite source to deposit graphene oxide and reduced graphene oxide layers on

J. Compos. Sci. 2023, 7, 309 2 of 13

conductive substrates [9]. Generally, methods utilized to produce graphene are multi-step, expensive, and have the potential to include impurities during fabrication and transfer to the target polymer matrix [5]. Moreover, the mixing of defect-free and inert pristine graphene with polymers is inhomogeneous and can lead to agglomeration in the matrix. Among these methods, melt processing shows the most potential for commercialization with certain limitations (poor dispersion and material degradation) [6].

Nosker and Lynch et al. invented a method that describes the fabrication process of a G-PMC formed by combining graphite and a thermoplastic polymer in a melt-processing method that applies a succession of shear strain events to the molten polymer phase, which exfoliates the graphite into graphene nanoflakes (GNFs) and distributes the GNFs uniformly within the polymer matrix [10–16]. The shear rate induces a shear stress that is higher than the interlayer shear strength of graphite in order to separate the graphene layers within the molten polymer. Thus, graphite is converted to GNFs within the polymer, GNFs are uniformly distributed within the polymer matrix, and there is ample opportunity for in situ functionalization between newly created GNF edges and the polymer (i.e., during processing, a fracture occurs across the graphene basal plane resulting in reactive edges available to bond with the surrounding polymer while no other impurities are present to bond with the GNF edges). Graphite is exfoliated to create GNF particles with a varying degree of graphene layers in each particle. The degree of exfoliation increases with mixing time during melt-processing (i.e., with increased exposure to shear strain events). This in situ shear exfoliation method does not create graphene as a stand-alone material. Rather, this in situ shear exfoliation method creates a nanocomposite with beneficial and tunable properties at a low cost.

In previous work using this in situ shear exfoliation method, 35 wt. % graphite was exfoliated within polyetheretherketone (PEEK) to create GNF-enhanced PEEK nanocomposites [17]. Morphology and X-ray diffraction results indicated surface crystallization of PEEK on GNF surfaces, very good planar adhesion, and size reduction of GNFs in both the c-axis direction and in diameter due to the fracture across the basal plane; spectroscopic analysis from Raman and XPS spectra indicated in situ formation of chemical bonding between created GNFs and PEEK, and mechanical property results showed a 400% increase in tensile modulus.

Here, we use this one-step, in situ shear exfoliation method to convert graphite into multilayer graphene directly within polysulfone and within polyvinylidene fluoride (PVDF) to prepare G-PSU and G-PVDF nanocomposites that perform as multifunctional sensor materials. PSU is a thermoplastic that contains a characteristic aryl group connected by sulfonyl and ether groups [18]. With different conductive fillers and in combination with different metals, PSU has been used as a humidity sensor, gas sensor, strain sensor, and biosensor [18–23]. However, the nanofiller that provides excellent functionalities to the composite is expensive and makes the resultant sensor economically less attractive. PVDF is a semi-crystalline thermoplastic polymer with favorable characteristics such as a low cost, good mechanical properties, resistance to chemicals, thermal stability, and unique pyroelectric and piezoelectric properties [24,25]. With enhanced properties, G-PSU and G-PVDF nanocomposites show promise as materials for many sensor applications.

Traditional sensors require a battery power supply to acquire signals in monitoring systems, which increases the complexity. Further, this battery-powered sensor cannot always be easily adjusted, and so may not be feasible to employ in hostile situations or for in vivo biomedical applications [26,27]. Thus, wireless sensing technology has become a viable feature for avoiding active electronics and has drawn a lot of attention in recent years. A passive resistive inductive capacitive (RLC) strain monitoring circuit based on flexible electronics with a wireless readout mechanism eliminates any active circuit elements in the implant. The method utilizes resonant frequency measurements with a network analyzer or impedance analyzer, where the readout system and sensor communicate wirelessly via electromagnetic inductive coupling. The sensor comprised a series RLC circuit with variable resistance and capacitance that changes with strain. The corresponding shift in RLC

network analyzer or impedance analyzer, where the readout system and sensor commentacate wirelessly via electromagnetic inductive coupling. The sensor comprised a series RLC circuit with variable resistance and capacitance that changes with strain. The correspondresorbifit ine flency symmetric weaks resistant records of the shures production sense and the sensor between the substitution of the sensor production of the sensor of

$$f_s = \frac{f_s}{2\pi\sqrt{L_sC_s}} \tag{1}$$
 In this study, we show the effects of in situ shear exfoliation of graphite into GNFs

In this study, we show the effects of in situ shear exfoliation of graphite into GNFs directly within PSU land PVDF during uniform shear restorations on shapting innocential directly within PSU land PVDF during tive properties (Figure 1) and Australia describe the circumstantial describe the circumstantial described by the properties of the shape of the circumstantial described to the properties in properties in the circumstantial described to the properties in the circumstant of the properties in the circumstant of the

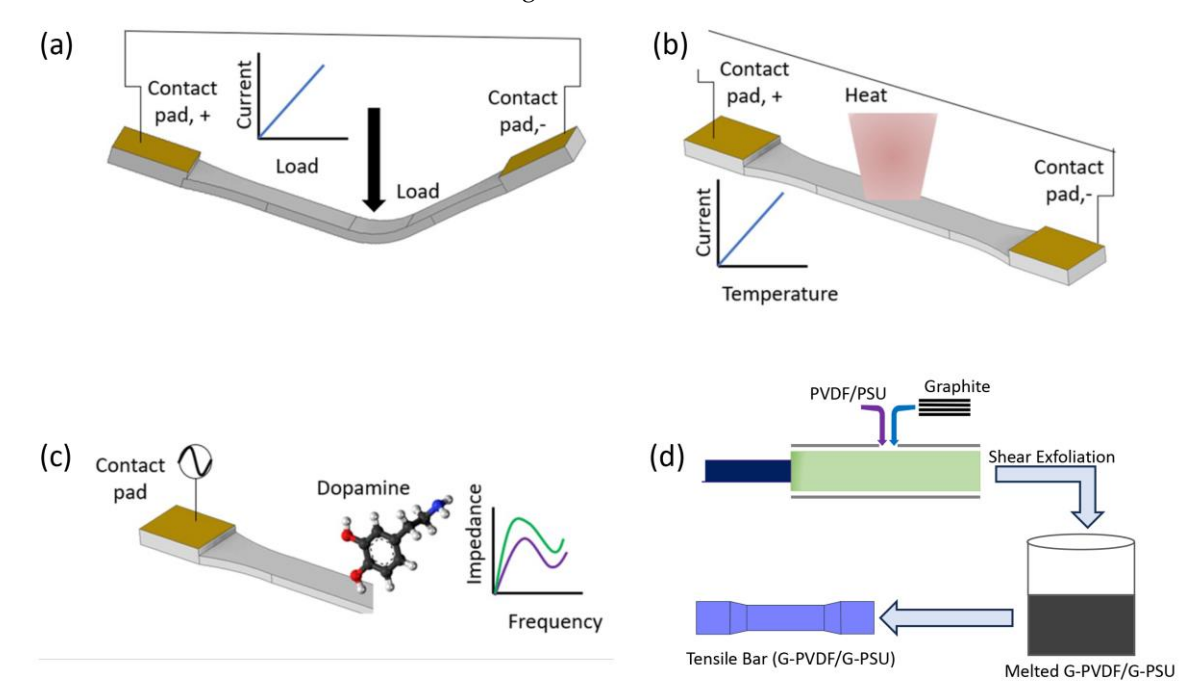


Figure 1. Schematic diagram representing multifunctional C-PME sensor. (a) Strain sensor, (b) temperature sensor, (c) electrockness electrockness and (d) sensor exclaiming process.

2. Materials and Methods 2. Materials and Methods

Mined graphite (Asbury Carbons mills grade 3627 with 99.2% purity and an averMined graphite (Asbury Carbons mills grade 3627 with 99.2% purity and an average diameter ranging from 250 to 300 µm) was combined with polysulfone (Udel® 1700, SolSolvay Advanced Polymers) to make G-PSU and with polyvinylidene fluoride (Kynar 720,
Yay Advanced Polymers) to make G-PSU and with polyvinylidene fluoride (Kynar 720,
Arkema) to make G-PVDF. This grade of PVDF is reported by Arkema to have a specific
Gravity of 1.77-1.79, a melting temperature of 165-172 °C, and tensile strength of 34-55
MPa. This grade of PSU has a specific gravity of 1.24, a melting temperature of 149 °C, and
tensile strength of 60.3 MPas a specific gravity of 1.24, a melting temperature of 149 °C,
and tensile strength of 70.3 MPas as a specific gravity of 1.24, a melting temperature of 149 °C,
and tensile strength of 70.3 MPas and tensile strength of 32-35
from 20 to 40 wt. % graphite in PSU in two 500 g batch sizes to help distribute the graphite
amongst PSU pellets, added to the hopper of a modified injection molding machine with a
unique screw design by Randcastle Extrusion Systems, Inc. (Cedar Grove, NJ, USA), and

J. Compos. Sci. **2023**, 7, 309 4 of 13

tensile specimens molded (ASTM D638 Type I with dimensions 3.4 mm by 12.5 mm by 165 mm and a gauge length of 70 mm), as shown in Figure 1d. Materials were processed under a dry nitrogen blanket at 100 RPM and at processing temperatures of approximately 360 °C. The stainless-steel mold temperature was set at 105 °C using a PID temperature controller. Prior to injection molding, PSU and graphite were placed in a furnace at 160 °C for more than 12 h to remove volatiles. The unique screw design imparts uniform shear to exfoliate graphene layers from the bulk-layered graphite material, converts graphite into graphene nanoflakes (GNFs) with various numbers of layers in the c-axis direction, and uniformly distributes GNFs within the PSU, in a similar manner to that described in the previous work [17].

G-PVDF nanocomposites were prepared using a Randcastle micro-batch mixer that imparts elongational flow, folding, and uniform shear to exfoliate graphite into GNFs within PVDF. Prior to melt-processing, PVDF was placed under vacuum for more than 4 h, and graphite was placed in a convection oven at 185 °C for approximately 12 h to remove volatiles. PVDF was added to the batch mixer using starve-feeding followed by the proper graphite concentration, and the components were mixed under a dry nitrogen environment at a processing temperature of approximately 204 °C (but varied slightly with concentration) for a mixing time of 90 min (after the graphite was added). The shear rate during processing is critical to allow exfoliation of nanoplatelets and to achieve uniform distribution of the nanofiller within the polymer matrix [28,29]. Thus, the target processing RPM was over 100 RPM in order to achieve sufficient shear stress to efficiently exfoliate graphite into GNFs and varied as 150, 120, 120, 200, and 15 RPM for 0, 5, 10, 20, and 30 wt. % GNFs in PVDF, respectively. The shear rate depends on RPM and the geometry of the processing machine. The corresponding shear rate was calculated for each starting graphite concentration in PVDF and is shown in Table 1. Notice that for 30 wt. % GNFs in PVDF, the machine was limited to 15 RPM due to increasing viscosity at this high concentration and the current (amp) limitation of this specific machine. The extrudate and bulk pieces from the batch mixer were grounded, placed in a vacuum to remove volatiles for more than 4 h, and molded into ASTM D638 Type V tensile specimens using a mini-molding machine.

Table 1. Batch mixer processing RPM and corresponding shear rates for each starting graphite concentration in PVDF.

% Graphite in PVDF	RPM	Shear Rate (1/s)
0	150	1202
5	120	962
10	120	962
20	200	1602
30	15	120

Material characterization of the G-PMCs included morphology, structure, thermal properties, and mechanical properties. Morphology was viewed using a Zeiss field emission scanning electron microscope (SEM). G-PSU and G-PVDF samples were cold fractured, mounted on typical aluminum studs with carbon black tape, and gold coated with a thickness of 5 nm. Raman data were collected using a Renishaw inVia reflex system with a 633 nm laser and 50× magnification, and the 40 wt. % G-PSU results are presented. Raman specimens were cut from the tensile specimens to approximate dimensions of 10 mm × 10 mm × 3 mm with the top surface investigated after polishing with a course grade emery paper. Thermogravimetric analysis (TGA) was performed using a TA Instrument Q5000 under a nitrogen atmosphere up to 1000 °C with a ramp rate of 5 °C/min and results for 35 wt. % G-PSU sample are presented. TGA Specimens were cut from tensile specimens having a mass of approximately 35.6 mg. Mechanical properties were determined using an MTS Qtest/25 Elite Controller. G-PSU samples were tested in flexural according to ASTM D790 at a crosshead speed of 1.34 mm/min. G-PVDF Type

J. Compos. Sci. **2023**, 7, 309 5 of 13

V specimens were tested in tension according to ASTM D638 using an extensometer to measure strain.

The electromechanical sensor capability of G-PSU and G-PVDF samples was tested by cyclically loading and unloading specimens in 3-point flexural loading using an Instron 5982 universal testing system while simultaneously monitoring the current as a function of time under a potential of 10 volts using a Keithley 2450 source measure unit. Cyclic loading of 40G-PSU was performed over 50 cycles at a 10 N load followed by 50 cycles at a 20 N load, and specimens were manually loaded and unloaded. For G-PVDF sensor testing, G-PVDF extrudate was compression molded into thin sheets and attached to a tensile bar composed of PEEK. The tensile bar was cyclically loaded, and the G-PVDF acted as the sensor to measure the resistance over time during the cyclic loading and unloading procedure. One loading cycle was approximately 1 min and 30 s, which included loading to 20 N (approximately 30 s), holding the 20 N load for 30 s, unloading to 0 N (instant de-load and manual force zero), and holding 0 N for 30 s.

Temperature sensor testing was performed on 40G-PSU, a high GNF concentration, since GNFs enhance thermal conductivity. Thus, 40~G-PSU specimens (dimensions according to ASTM D 638 Type 1 tensile specimens) were subject to heating with a heat gun up to 80~C and cooling down to 10~C by evaporating liquid nitrogen under the sample while monitoring the temperature with a thermal imager (RSE600, Fluke Corporation, Everett, WA, USA) and simultaneously measuring the change in resistance using Keithley 2450 source measure unit under the voltage potential of 10~V.

To monitor the sensor data wirelessly, a passive wireless resonant circuit was fabricated, and the bending data were obtained from the resonant frequency. For the inductor coil of the sensor and readout system, a copper coil with a wire diameter of 1.5 mm was used. The coil inductances of the sensor and readout side were 11.6 μ H and 11 μ H, respectively. The frequency response of the sensor was remotely monitored through the minimum of the input return loss (S11) in the readout device using an HP8752C network analyzer.

Electrochemical sensing was performed using a three-electrode system where the working electrode was G–PSU (or G–PVDF, respectively), silver wire was the counter electrode, and platinum wire was the reference electrode. The dimensions of the G–PSU and G–PVDF specimens were $10 \text{ mm} \times 10 \text{ mm} \times 1.5 \text{ mm}$. Electrochemical impedance spectroscopy (EIS) was used to evaluate the performance of G–PSU and G–PVDF as electrochemical sensors for dopamine detection. To evaluate the performance of G–PVDF and G–PSU as electrochemical sensors, we used the experimental setup shown in Figure S2. We measured impedance with $\text{Fe}^{2+}/\text{Fe}^{3+}$ redox couple as analytes. Then, dopamine was added with concentrations of 1 mM, 2 mM, and 3 mM while running an EIS test in the frequency range from 10 to 105 Hz.

3. Results and Discussion

3.1. Material Characterization

The morphology of 40G-PSU is displayed in Figure 2a,b, with SEM images showing GNFs uniformly distributed in the polymer matrix. No filler agglomeration was observed from the SEM images. This uniform distribution of GNFs within PSU is similar to our previous work investigating in situ exfoliation of graphite into GNFs within an Ecoflex 00-30 using an infrared thermography approach [30,31]. The original graphite flake diameter was $\sim 300~\mu m$; however, the GNF size measured in SEM images is $\sim 10~\mu m$, indicating a shear-induced fracture across the basal plane resulting in edge sites that are available to form covalent bonds with surrounding polymer molecules. The conformal coating of the GNFs by the polymer indicates strong interfacial adhesion between them (Figure 2b). The morphology of 30 wt. % GNFs in PVDF is shown in the SEM micrographs at different magnifications in Figure 2c,d. At high magnification $(20,000\times)$, the particle–matrix interaction between GNFs and PVDF is visible in Figure 2d. There is very good adhesion between GNF planar surfaces and the PVDF matrix, as well as between visible GNF edges and the PVDF matrix. There is some gap spacing between GNFs and PVDF, which is due to the

GNFs by the polymer indicates strong interfacial adhesion between them (Figure 2b). The morphology of 30 wt. % GNFs in PVDF is shown in the SEM micrographs at different magnifications in Figure 2c,d. At high magnification (20,000×), the particle–matrix interaction between GNFs and PVDF is visible in Figure 2d. There is very good adhesion between GNF planar surfaces and the PVDF matrix, as well as between visible GNF edges and the PVDF matrix. There is some gap spacing between GNFs and PVDF, which is due published the dulting colding activing using the particle particle and the published colding activing using the particle particle and the published colding activities are coldinately activities.

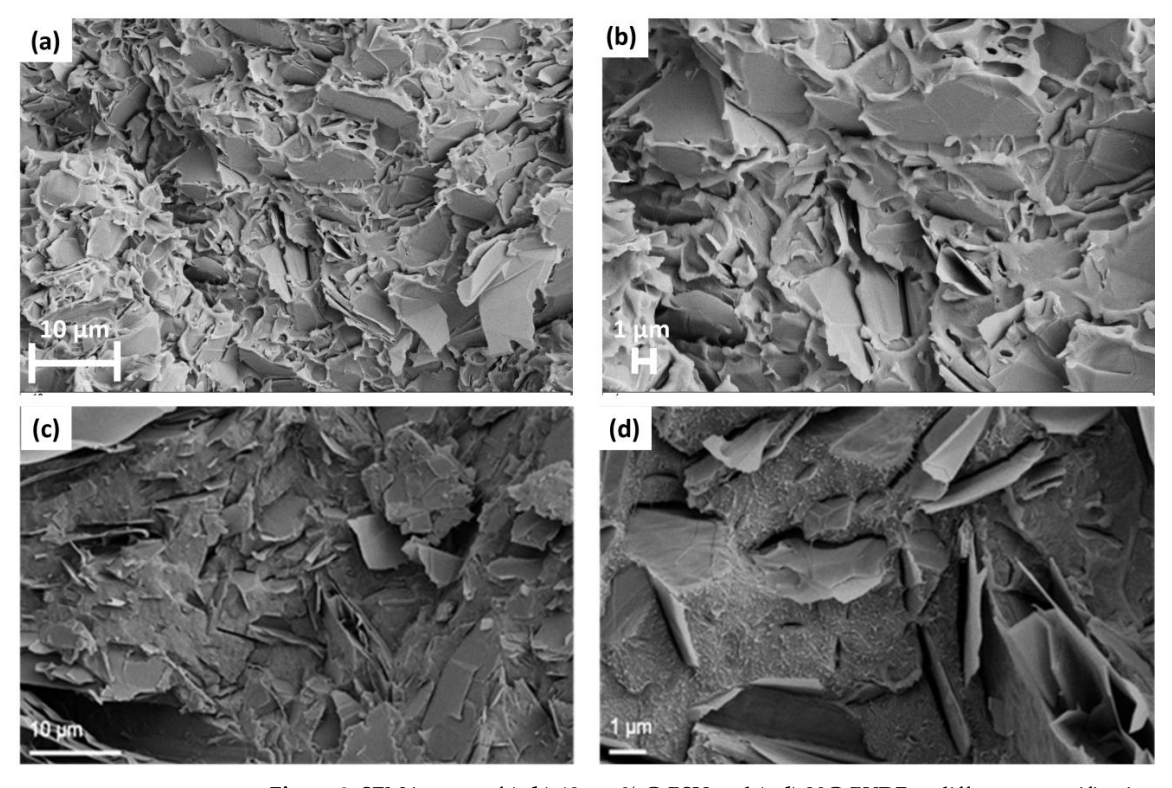


Figure 2. SEM images of (a,b) 40 wt. % G-PSU and (c,d) 30G-PVDF at different magnifications. Figure 2. SEM images of (a,b) 40 wt. % G-PSU and (c,d) 30G-PVDF at different magnifications.

The Raman spectrum of 40 wt. %, G-PSU is presented in Figure 3a. Typical peaks associated with graphene can be observed at ~1350 cm for the D band, ~150 cm for the peaks associated with graphene can be observed at ~1350 cm for the D band. The Intensity ratio 80 cm for the peaks associated with graphene can be observed at ~1350 cm for the D band. The Intensity ratio 80 cm for the point of the peak of

Compos. Sci. 2023, 7, x FOR PEER REVIEW

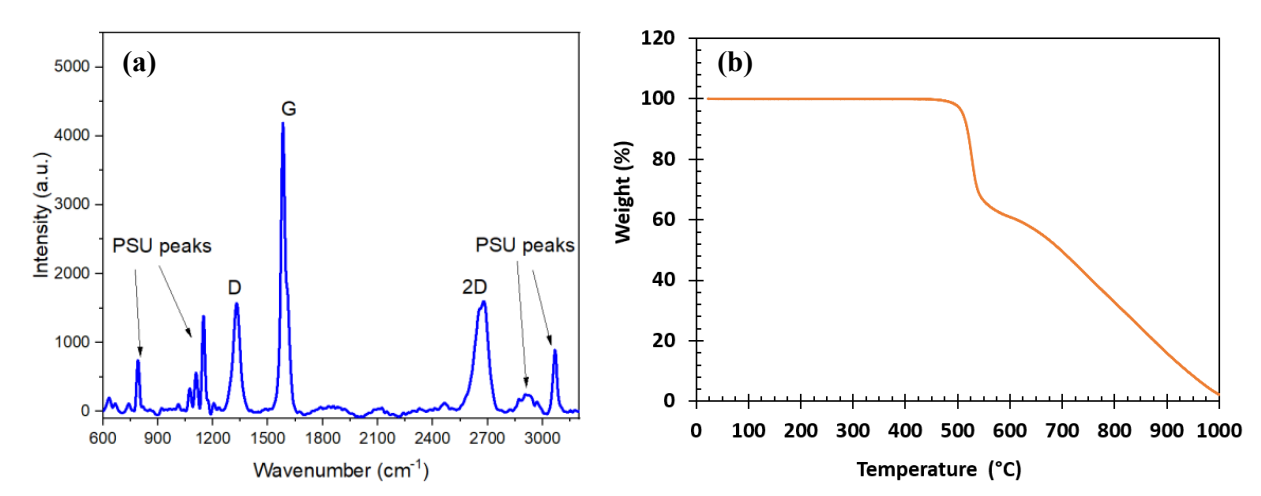


Figure 3. (a) Raman spectrum of 40 wt. % G–PSU and (b) TGA of 35 wt. % G–PSU. **Figure 3.** (a) Raman spectrum of 40 wt. % G–PSU and (b) TGA of 35 wt. % G–PSU.

Flexural mechanical properties are shown for G-PSU in Figure 4a,b, and tensile mechanical properties are shown for G-PVDF in Figure 4c,d. The flexural modulus increases with GNF concentration in PSU by 67%, 130%, and 190% for 20, 30, and 40 wt. % GNFs in

J. Compos. Sci. **2023**, 7, 309 7 of 13 **Figure 3. (a)** Raman spectrum of 40 wt. % G-PSU and **(b)** TGA of 35 wt. % G-PSU.

Flexural mechanical properties are shown for G-PSU in Figure 4a,b, and tensile mechanical properties are shown for G-PSU in Figure 4a,b, and tensile mechanical properties are shown for G-PSU in Figure 4a,b, and tensile mechanical properties are shown for G-PSU in Figure 4a,b, and the flexural mechanical properties are shown for G-PSU in Figure 4a,b, and 40 with G-PSU in Figure 4b, and 40 with G-PSU in Figure 4b, and 40 with G-PSU in Figure 4b, and 4b, and the tensile modulus increases with G-PSU in G-PSU in Figure 4a,b, and the tensile modulus increases with G-PSU in G-PSU

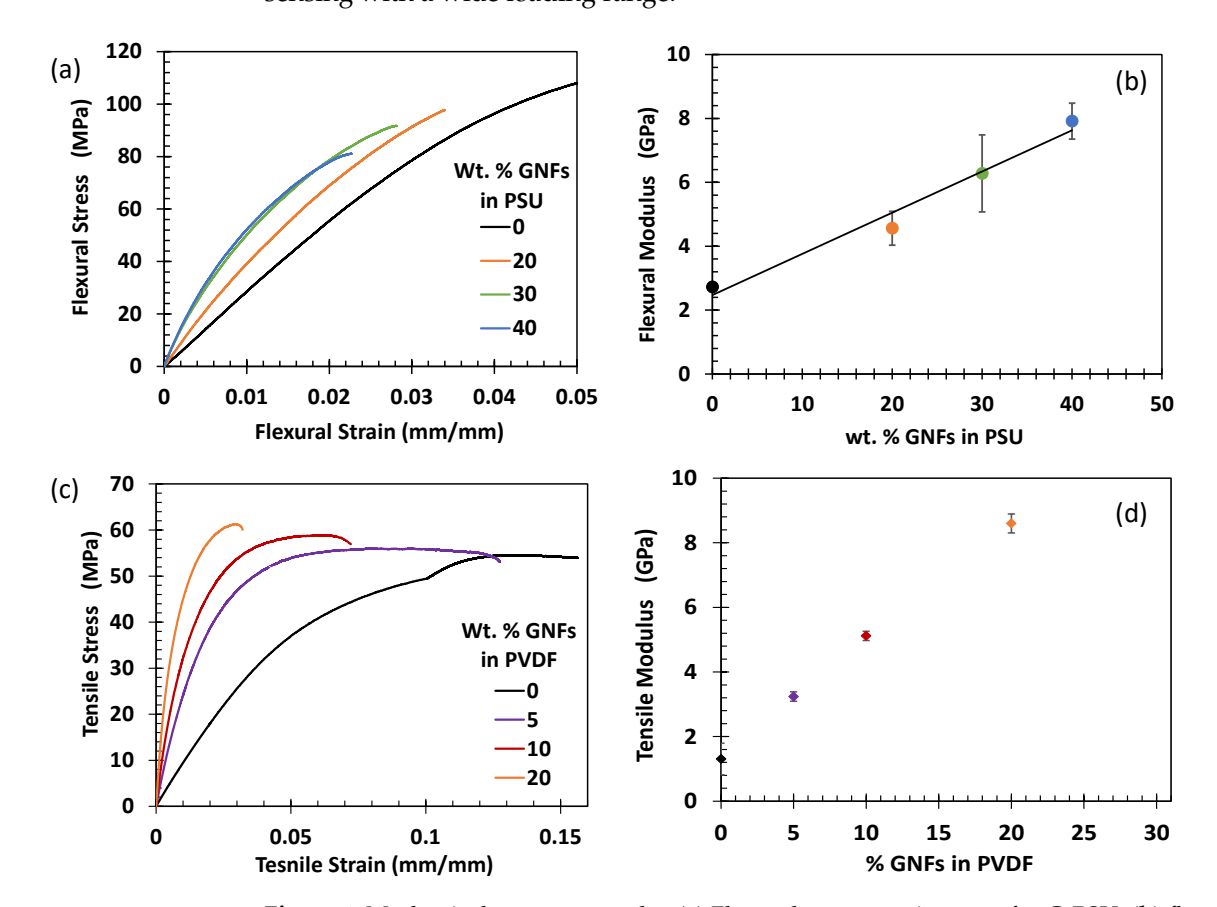


Figure 4: Mechanical property results: ((a) Flexural stress-strain awardo CG-PSU, (b) flexural modulus for G-PVDF, and (d) tensile modulus for G-PVDF.

3.2. Electromechanical Strain Sensing

Under an external load, the distance between graphene in the composite and the structure of the hexagonal honeycomb will change, resulting in a change in resistance and therefore current flow through the composite sensor [34]. Electrons tunnel or hop from one graphene flake to another (if the filler content is above the percolation threshold in the composite), and that is why the change in distance between graphene flakes changes the resistance to electron flow [31].

To determine the repeatability of the sensor strain performance, a 40 wt. % G-PSU sample was subjected to 10 and 20 N load (within the elastic regime) 50 times, as shown in Figure 5a. The experimental setup for this test is shown in Figure S4. An ASTM D 638 Type I sample with silver paint contact pads and the copper electrode was subjected to cyclic loads that were manually operated. Results show the consistent amplitude of resistance change for 50 cycles at 10 N load and 20 N load with a slight variation due to the manual loading technique, indicating the durability of the 40~G-PSU sensors during long service life. The sensor showed reversible and self-sensing behavior, which has been described as an advantage of 2D nanofillers (e.g., graphene) vs. 1D nanofillers (e.g.,

Type I sample with silver paint contact pads and the copper electrode was subjected to cyclic loads that were manually operated. Results show the consistent amplitude of resistance change for 50 cycles at 10 N load and 20 N load with a slight variation due to the manual loading technique, indicating the durability of the 40 G-PSU sensors during long service life. The sensor showed reversible and self-sensing behavior, which has been described as an advantage of 2D nanofillers (e.g., graphene) vs. 1D nanofillers (e.g., CNT) [35]. The gauge factor (percentage change in resistance vs. change in strain) for the cyclic costing with the 20 Algeric was found to be 27 and in resistance vs. change in strain) for the cyclic costing with the 20 Algeric was found to be 27 and in resistance vs. change in strain) for the cyclic costing with the 20 Algeric was found to be 27 and in resistance vs. change in strain) for the cyclic costing with the 20 Algeric was found to be 27 and in resistance vs. change in strain) for the cyclic costing with the constitution of the cyclic cost in particles with the cost of the cyclic cost in the cyclic cost in the cyclic cost in the cyclic c

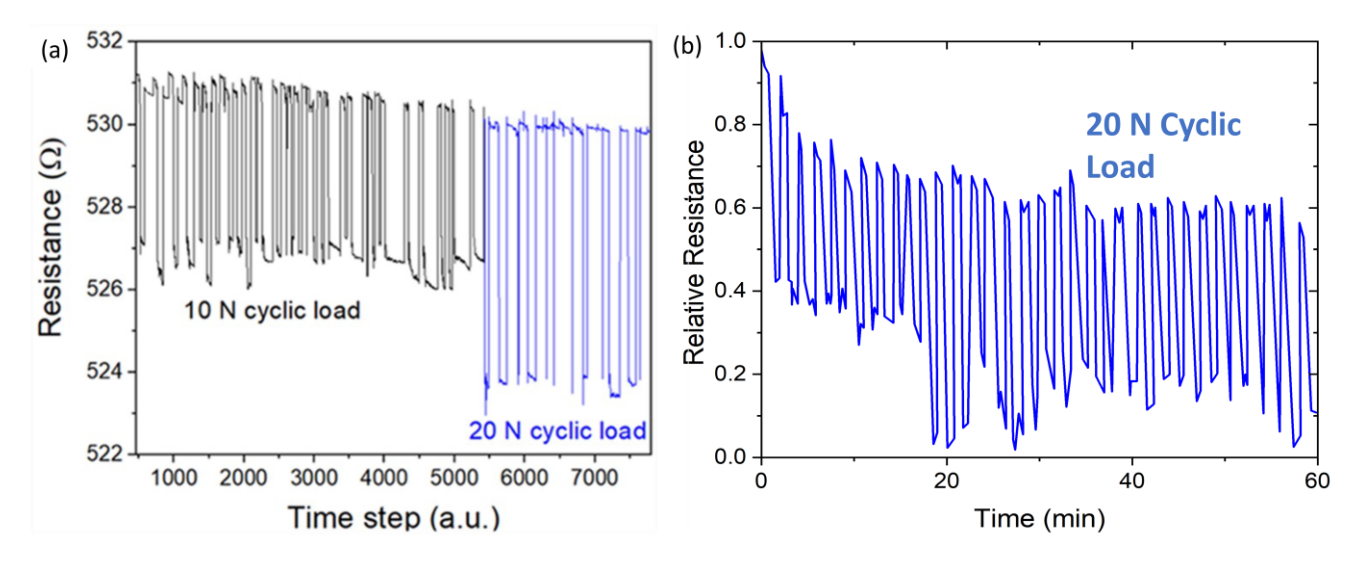


Figure 5. (a) Manual cyclic loading of 40 wt. % G-PSU sample undergoing 50 cycles of 10 N and them 20 N loads during the same test. Due to manual loading the undergoing to cycles of 10 N and then 20 N loads during the same test. Due to manual loading the time between each cycle was not 20 N loads during the same test. Due to manual loading the time between each cycle was not controlled. (b) Cyclic loading of G-PVDF for 35 loading/unloading cycles of 20 N load. trolled. (b) Cyclic loading of G-PVDF for 35 loading/unloading cycles of 20 N load.

3.3. Temperature Sensing

3.3. Tamperature Sensing temperature change with time, as well as thermal images, are presented for it to consider the interpretation of the presented for it to consider the interpretation of the presented for its consideration of the presented for its consideration of the sense of the sens

Since G-PSU is stable up to 500 °C (3b), the potential of the sensor under different temperature regimes and harsh conditions (like corrosive environments) will be tested in the future. Polysulfone is already a widely accepted material used in the automotive industry (steering column lock switches, relay insulators, and pistons) and in medical equipment (nebulizers and dialysis components) [8]. Therefore, G-PSU, with its excellent temperature sensing properties, can be a suitable strain and temperature sensor for the automotive, medical, and aerospace industries. Additionally, the nanocomposites' good electrical and thermal properties and chemical stability make them an economically viable material for molded interconnect devices for consumer electronic, telecommunication, automotive, and medical technologies, as well as lightweight structural parts for collaborative robots (i.e., Cobots).

the same rate as the temperature, indicating minimal hysteresis (Figure 8). The hysteresis the same rate as the temperature, indicating minimal hysteresis (Figure 8). The hysteresis (difference in resistance change at the same temperature during heating and subsequent (difference in resistance change at the same temperature during heating and subsequent cooling) can be as high as ~20%, whereas in our case it was only 0.42% [23]. Thermal imcooling) can be as high as ~20%, whereas in our case it was only 0.42% [23]. Thermal images (from thermal video recording during the entire test) show a uniform temperature ages from thermal video recording during the entire test) show a uniform temperature profile across the sample area being heated, indicating uniform dispersion of the nanofillers in the polymer composite (Figures 7b and 8b) [30,31].

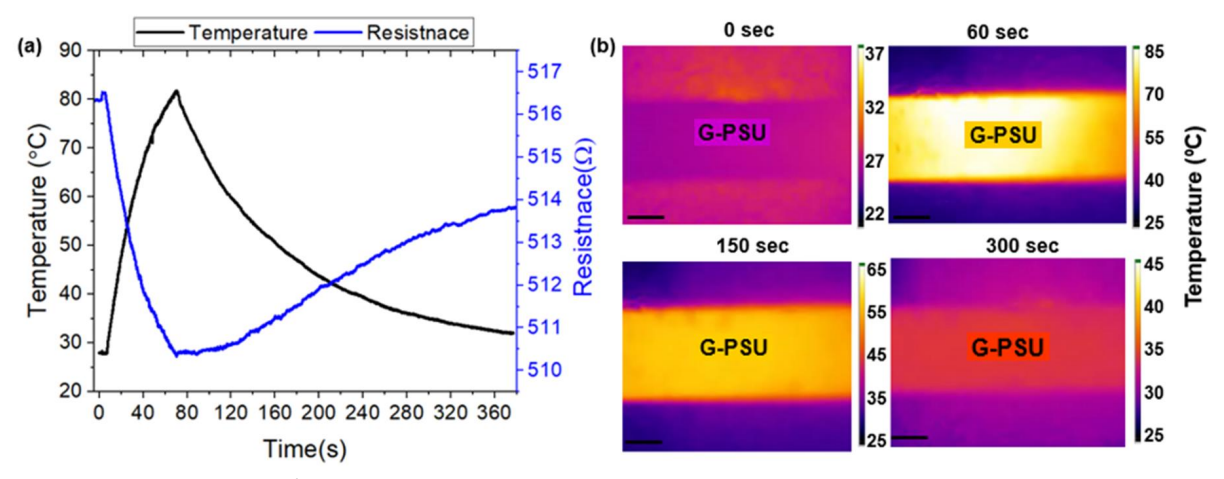


Figure 6.Thermal sensor heating test of GPSDs (a) Blots showing a change in temperature with figure 6. Thermal sensor heating test of GPSDs (a) Blots showing a change in temperature with time uning heating and recovery in the bottom and corresponding spectrical resistance change on top, and (b) corresponding thermal images captured during the test. The excurrence of the corresponding thermal images captured during the test.

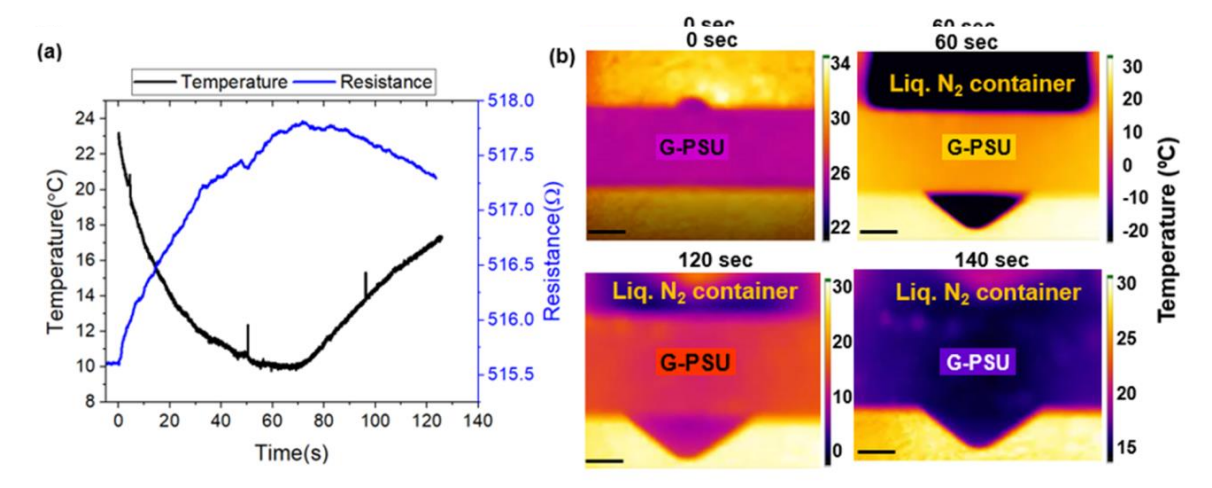


Figure 7. Thermal sensor cooling tests of G-PSIJ (a) Plots showing a change in temperature with J. Compos. Sci. 2023, 7, × FOR PEER Implication of the potton and corresponding electrical resistance change on the potton and corresponding the main integer appured that it is a proper to the proper of the property of the property

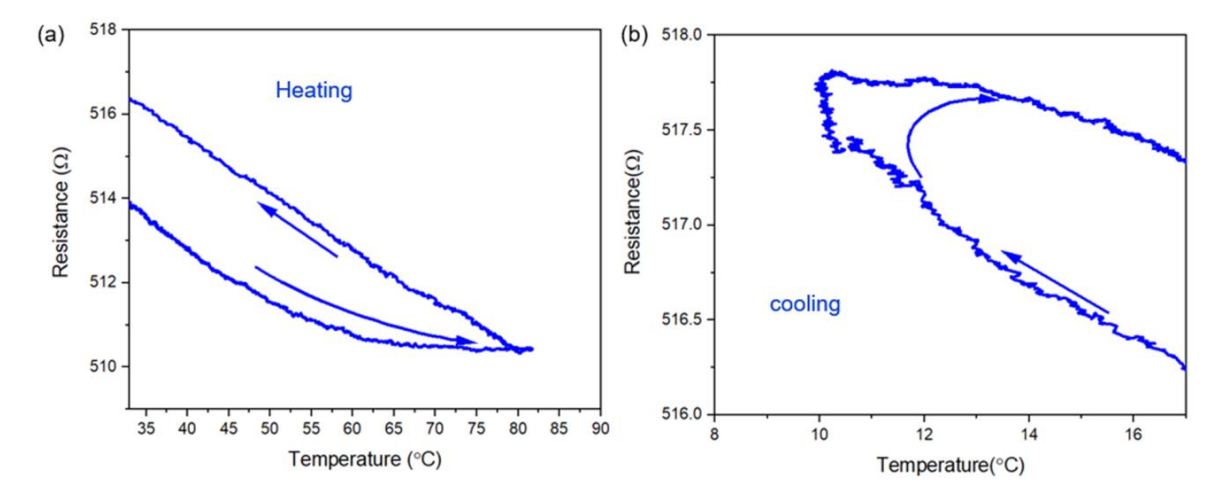


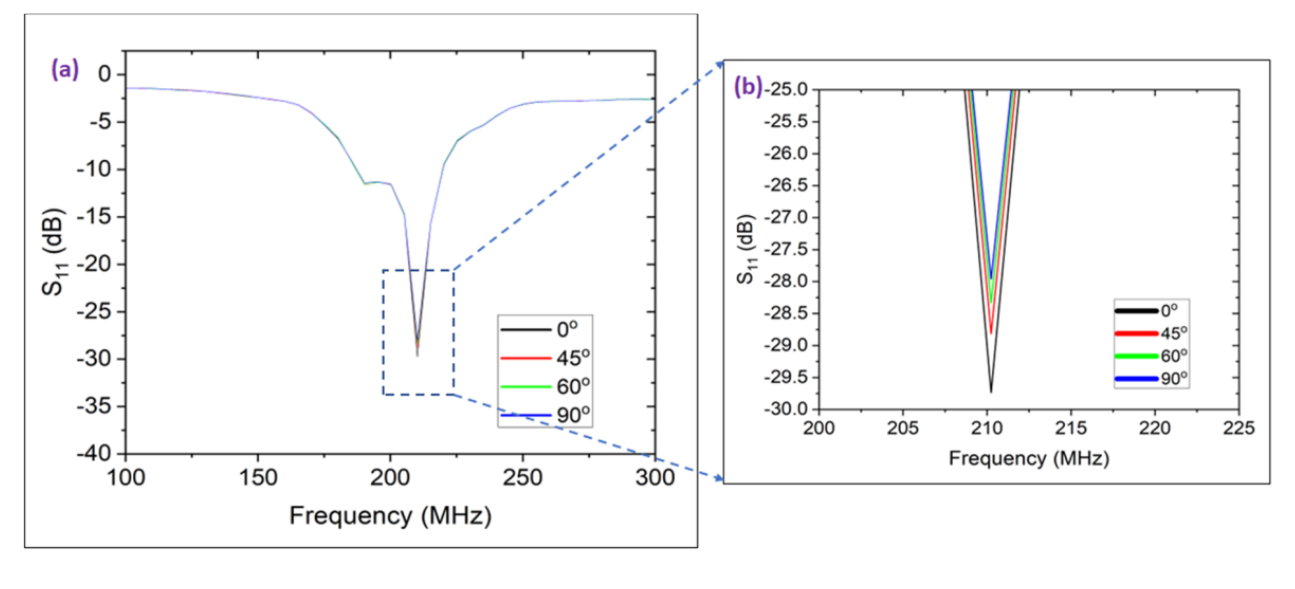
Figure 8. Hysteresis of G-PSU sensor during (a) heating and (b) cooling. Arrows indicate progression of data collection during application of thermal input (heating/cooling) and after removal of the application during application of thermal input (heating/cooling) and after removal of the application during application of the application of the application during application of the application of the input, during which the sample returns back to its initial thermal state.

Since G-PSU is stable up to 500 °C (3b), the potential of the sensor under different temperature regimes and harsh conditions (like corrosive environments) will be tested in the future. Polysulfone is already a widely accepted material used in the automotive industry (steering column lock switches, relay insulators, and pistons) and in medical equipment (nebulizers and dialysis components) [8]. Therefore, G-PSU, with its excellent temperature sensing properties, can be a suitable strain and temperature sensor for the auto-

3.4. Wireless Sensing

Due to bending at different angles around a roller with a diameter of 43 mm, a change in capacitance and resistance was observed in the sensor. Input return loss (S11) with frequency for bending at different angles of the 40 wt. % G-PSU and 30 wt. % G-PVDF are shown in Figure 9. The resonant frequencies of the G-PSU and G-PVDF remain closely in the range ~212 MHz and ~429 MHz, respectively, while the signal amplitude of them gradually decreases due to the bending from 0° to 90° . The decrease in amplitude rsignifies the change in sensor resistance and the small peak shift was due to the change $_{
m 0f}$ $_{
m 14}$

J. Compos. Sci. 2023, 7, x FOR PEER REV in sensor capacitance. As a result, the passive wireless RLC circuit enabled reliable signal detection capacitance.



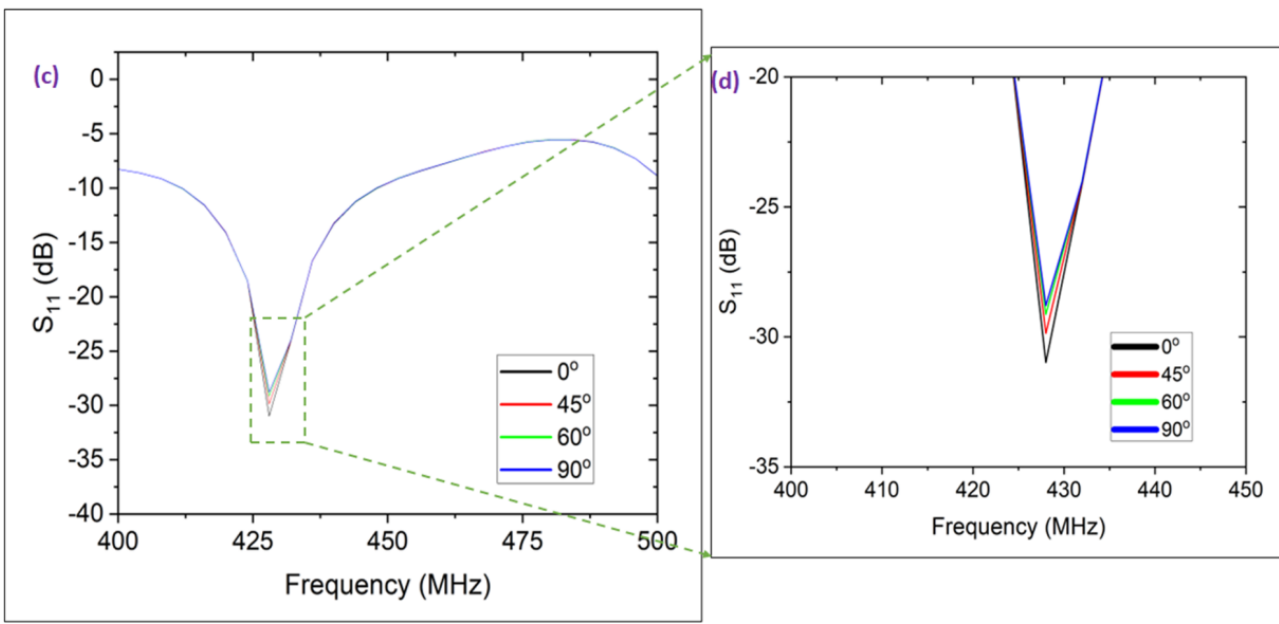


Figure 5. Frequency response curve sensor due to bending at different angles for (a) G-BSU, (b) enlarged view of (a), (c) PV DFV on d. (d) (an larged view of (c)).

3.53 Electrochanian Sensing

The resulting Nyquist diagrams for G-PSU (40 wt. %) and G-PVDF (30 wt. %) (Figure followed by a straight line for the diffusion-limited electron transfer process at lower frequencies. The equivalent circuit is obtained by the best-fitting model (the Randles circuit and its representing Nyquist plot are shown in Figure 10c,d) to obtain the charge transfer resistance. It is evident that the semi-circular region's width increases with rising dopamine levels due to polarization resistance. In the case of C-PSII, the electron charge trans

at lower frequencies. The equivalent circuit is obtained by the best-fitting model (the Randles circuit and its representing Nyquist plot are shown in Figure 10c,d) to obtain the charge transfer resistance. It is evident that the semi-circular region's width increases with rising dopamine levels due to polarization resistance. In the case of G–PSU, the electron charge transfer resistance for Fe^{2+}/Fe^{3+} solution is 119 Ω , for 1 mM, 2 mM, and 3 mM dopamine concentrations and the electron charge transfer resistance is 40.8 Ω , 52 Ω and 55.1 Ω , respectively. In the case of G–PVDF, for Fe^{2+}/Fe^{3+} redox couple, 1 mM, 2 mM, and 3 mM dopamine concentrations the electron charge transfer resistance is 55.8 Ω , 128 Ω , 158 Ω , and 164 Ω , respectively. The calculated limit of detection (LOD) is 3.671 mM and 4.515 mM for G–PSU and G–PVDF, respectively.

Compos. Sci. 2023, 7, x FOR PEER REVIEW

Ferri Ferro solution with 1mM dopamine Ferri Ferro solution with 2mM dopamine (a) (b) rri Ferro solution with 3mM dopamine (U),Z- $-Z'(\Omega)$ 40 Ferri ferro solution Ferri ferro solution with 1mM dopamine Ferri ferro solution with 2 mM dopamine Ferri ferro solution with 3 mM dopamine 20 10 150 250 $Z'(\Omega)$ $Z'(\Omega)$ Z_{imag} (d) (c) $\omega = 1/(R_{ct} * C_{dl})$ $\boldsymbol{R}_{\text{ct}}$ Rs

Figure 10. Electrical impedance spectroscopy analysis for different dopamine concentrations; Figure 10. Electrical impedance spectroscopy analysis for different dopamine concentrations; (a) G-PSU (b) G-PVDF, (c) Randles equivalent circuit, and (d) the representing equivalent Nyquist plot.

4. Conclusions

4. Conclusions helicion, by in situ exfoliation of graphite into graphene within PSU and PVDF

In edicities work by in left extrination of graptine had graphene with a property of PSU and PVDF matrices, we were able to fabricate a multimedional material especially suitable for strain, electrical and thermal properties. A G-PSU nanocomposite with 35-40 wt. "fittler, dopamine, wireless, and temperature sensing due to GNF enhancement of PSU and PVDF loading was able to detect strain in the elastic regime with a gauge factor of 27 and minimal electrical and thermal properties. A G-PSU nanocomposite with 35-40 wt. "fittler, dopamine, wireless, and temperature sensing due to GNF enhancement of PSU and PVDF loading was able to detect strain in the elastic regime with a gauge factor of 27 and minimal electrical and thermal properties. A G-PSU nanocomposite with a gauge factor of 27 and minimal electrical and thermal properties and electrical sension. Composite factor of 27 and minimal electrical sension of the electrical sension of electrical sension of electrical sension of electrical sension of the electrical sension of the electrical sension of the millimolar range. We believe that this research will open the door for commercially viable electrically and thermally conductive graphene thermoplastic nanocomposites with uniform nanofiller dispersion and distribution for application in different industries such as the automotive, medical,

conductive graphene thermoplastic nanocomposites with uniform nanofiller dispersion and distribution for application in different industries such as the automotive, medical, aerospace, robotics, consumer electronics, and telecommunications industries.

5. Patents

U.S. Patent Application Reference: Lynch-Branzoi, Jennifer K.; Ashraf, Ali. Conductive Polymer Nanocomposites Enhanced with In Situ Formation of 2D Nanoparticles for Structural Sensors and Smart Materials, US 2022/0112340, 14 April 2022.

Supplementary Materials: The following supporting information can be downloaded at: https://www.mdpi.com/article/10.3390/jcs7080309/s1, Figure S1: Schematic of a passive wireless sensor with a readout system; Figure S2: Experimental setup for electrochemical sensing of dopamine with G–PSU and G–PVDF; Figure S3: First heating curve; Figure S4: Experimental setup used for cyclic loading test; Table S1: Thermal property results for G–PVDF obtained using a DSC.

Author Contributions: Conceptualization, J.K.L.-B. and A.A.; methodology, J.K.L.-B. and A.A.; formal analysis, E.C., M.A.R. and D.G.; investigation, E.C., M.A.R. and D.G.; resources, J.K.L.-B., N.I. and A.A.; writing—original draft preparation, A.A., E.C., M.A.R. and D.G.; writing—review and editing, J.K.L.-B.; supervision, J.K.L.-B. and A.A. All authors have read and agreed to the published version of the manuscript.

Funding: Some of this research was funded by the National Science Foundation (NSF) under grant number ERI 2138574.

Data Availability Statement: The data that support the findings of this study are available from the corresponding author upon reasonable request.

Acknowledgments: The authors gratefully acknowledge the Materials Science and Engineering Department at Rutgers University for providing equipment and facilities for this research.

Conflicts of Interest: The authors declare no conflict of interest.

References

- 1. Boland, C.S.; Khan, U.; Backes, C.; O'Neill, A.; McCauley, J.; Duane, S.; Shanker, R.; Liu, Y.; Jurewicz, I.; Dalton, A.B. Sensitive, high-strain, high-rate bodily motion sensors based on graphene–rubber composites. *ACS Nano* **2014**, *8*, 8819–8830. [CrossRef]
- 2. Amjadi, M.; Kyung, K.U.; Park, I.; Sitti, M. Stretchable, skin-mountable, and wearable strain sensors and their potential applications: A review. *Adv. Funct. Mater.* **2016**, *26*, 1678–1698. [CrossRef]
- 3. Balaji, R.; Sasikumar, M. Graphene based strain and damage prediction system for polymer composites. *Compos. Part A Appl. Sci. Manuf.* **2017**, 103, 48–59. [CrossRef]
- 4. Han, S.; Chand, A.; Araby, S.; Cai, R.; Chen, S.; Kang, H.; Cheng, R.; Meng, Q. Thermally and electrically conductive multifunctional sensor based on epoxy/graphene composite. *Nanotechnology* **2019**, *31*, 075702. [CrossRef] [PubMed]
- 5. Jang, H.; Park, Y.J.; Chen, X.; Das, T.; Kim, M.S.; Ahn, J.H. Graphene-based flexible and stretchable electronics. *Adv. Mater.* **2016**, 28, 4184–4202. [CrossRef]
- 6. Papageorgiou, D.G.; Kinloch, I.A.; Young, R.J. Graphene/elastomer nanocomposites. Carbon 2015, 95, 460–484. [CrossRef]
- 7. Sadasivuni, K.K.; Ponnamma, D.; Thomas, S.; Grohens, Y. Evolution from graphite to graphene elastomer composites. *Prog. Polym. Sci.* **2014**, *39*, 749–780. [CrossRef]
- 8. Liu, F.; Wang, C.; Sui, X.; Riaz, M.A.; Xu, M.; Wei, L.; Chen, Y. Synthesis of graphene materials by electrochemical exfoliation: Recent progress and future potential. *Carbon Energy* **2019**, *1*, 173–199. [CrossRef]
- 9. Khakpour, I.; Rabiei Baboukani, A.; Allagui, A.; Wang, C. Bipolar exfoliation and in situ deposition of high-quality graphene for supercapacitor application. *ACS Appl. Energy Mater.* **2019**, *2*, 4813–4820. [CrossRef]
- 10. Nosker, T.J.; Lynch-Branzoi, J.K.; Hendrix, J.W.; Kear, B.H.; Chiu, G.; Tse, S. Covalent Conjugates of Graphene Nanoparticles and Polymer Chains and Composite Materials Formed Therefrom. US 11479652, 25 October 2022.
- 11. Nosker, T.J.; Lynch-Branzoi, J.K.; Kear, B.H.; Hendrix, J.W.; Chiu, G. Graphene-reinforced polymer matrix composites. US 11225558, 18 January 2022.
- 12. Nosker, T.J.; Lynch-Branzoi, J.K.; Kear, B.H.; Hendrix, J.W.; Chiu, G. In Situ Exfoliation Method to Fabricate a Graphene-Reinforced Polymer Matrix Composites. US 11174366, 16 November 2021.
- 13. Nosker, T.; Lynch, J.; Hendrix, J.; Kear, B.; Chiu, G.; Tse, S. In Situ Exfoliation Method to Fabricate A Graphene-Reinforced Polymer Matrix Composite. US 11098175, 24 August 2021.
- 14. Nosker, T.; Lynch, J.; Kear, B.; Hendrix, J.; Chiu, G. In Situ Exfoliation Method to Fabricate a Graphene-Reinforced Polymer Matrix Composite. US 10253154, 9 April 2019.

15. Nosker, T.; Lynch, J.; Hendrix, J.; Kear, B.; Chiu, G.; Tse, S. In situ exfoliation method to fabricate a graphene-reinforced polymer matrix composite (G–PMC). US 9896565, 20 February 2018.

- 16. Lynch-Branzoi, J.K.; Nosker, T.J.; Kear, B.H.; Chang, C.T. Use of Graphene-Polymer Composites to Improve Barrier Resistance of Polymers to Liquid and Gas Permeants. US 11479653, 25 October 2022.
- 17. Lynch-Branzoi, J.K.; Ashraf, A.; Tewatia, A.; Taghon, M.; Wooding, J.; Hendrix, J.; Kear, B.H.; Nosker, T.J. Shear exfoliation of graphite into graphene nanoflakes directly within polyetheretherketone and a spectroscopic study of this high modulus, lightweight nanocomposite. *Compos. Part B Eng.* **2020**, *188*, 107842. [CrossRef]
- 18. Ciobanu, M.; Marin, L.; Cozan, V.; Bruma, M. Aromatic polysulfones used in sensor applications. *Rev. Adv. Mater. Sci.* **2009**, 22, 89–96.
- 19. Ordóñez, S.S.; Fàbregas, E. New antibodies immobilization system into a graphite–polysulfone membrane for amperometric immunosensors. *Biosens. Bioelectron.* **2007**, 22, 965–972. [CrossRef] [PubMed]
- 20. Bautista-Quijano, J.; Avilés, F.; Aguilar, J.; Tapia, A. Strain sensing capabilities of a piezoresistive MWCNT-polysulfone film. *Sens. Actuators A Phys.* **2010**, *159*, 135–140. [CrossRef]
- 21. Sánchez, S.; Pumera, M.; Cabruja, E.; Fàbregas, E. Carbon nanotube/polysulfone composite screen-printed electrochemical enzyme biosensors. *Analyst* **2007**, *132*, 142–147. [CrossRef] [PubMed]
- 22. Sánchez, S.; Pumera, M.; Fàbregas, E.; Bartrolí, J.; Esplandiu, M.J. Carbon nanotube/polysulfone soft composites: Preparation, characterization and application for electrochemical sensing of biomarkers. *Phys. Chem. Chem. Phys.* **2009**, *11*, 7721–7728. [CrossRef]
- 23. Cen-Puc, M.; Pool, G.; Oliva-Avilés, A.; May-Pat, A.; Avilés, F. Experimental investigation of the thermoresistive response of multiwall carbon nanotube/polysulfone composites under heating-cooling cycles. *Compos. Sci. Technol.* **2017**, 151, 34–43. [CrossRef]
- 24. He, F.; Fan, J.; Lau, S. Thermal, mechanical, and dielectric properties of graphite reinforced poly (vinylidene fluoride) composites. *Polym. Test.* **2008**, 27, 964–970. [CrossRef]
- 25. An, N.; Liu, S.; Fang, C.; Yu, R.; Zhou, X.; Cheng, Y. Preparation and properties of β-phase graphene oxide/PVDF composite films. *J. Appl. Polym. Sci.* **2015**, 132, 41577. [CrossRef]
- 26. Boutry, C.M.; Chandrahalim, H.; Streit, P.; Schinhammer, M.; Hänzi, A.C.; Hierold, C. Characterization of miniaturized RLC resonators made of biodegradable materials for wireless implant applications. *Sens. Actuators A Phys.* **2013**, *189*, 344–355. [CrossRef]
- 27. Kananian, S.; Alexopoulos, G.; Poon, A.S. Robust Wireless Interrogation of Fully-Passive RLC Sensors. *IEEE Trans. Circuits Syst. I Regul. Pap.* **2022**, *69*, 1427–1440. [CrossRef]
- 28. Li, Y.; Shimizu, H. Toward a stretchable, elastic, and electrically conductive nanocomposite: Morphology and properties of poly [styrene-b-(ethylene-co-butylene)-b-styrene]/multiwalled carbon nanotube composites fabricated by high-shear processing. *Macromolecules* **2009**, 42, 2587–2593. [CrossRef]
- 29. Rath, T.; Li, Y. Nanocomposites based on polystyrene-b-poly (ethylene-r-butylene)-b-polystyrene and exfoliated graphite nanoplates: Effect of nanoplatelet loading on morphology and mechanical properties. *Compos. Part A Appl. Sci. Manuf.* **2011**, 42, 1995–2002. [CrossRef]
- 30. Rahman, M.A.; Rahman, M.M.; Ashraf, A. Automatic dispersion, defect, curing, and thermal characteristics determination of polymer composites using micro-scale infrared thermography and machine learning algorithm. *Sci. Rep.* **2023**, *13*, 2787. [CrossRef]
- 31. Ashraf, A.; Jani, N.; Farmer, F.; Lynch-Branzoi, J.K. Non-destructive investigation of dispersion, bonding, and thermal properties of emerging polymer nanocomposites using close-up lens assisted infrared thermography. MRS Adv. 2020, 5, 735–742. [CrossRef]
- 32. Backes, C.; Paton, K.R.; Hanlon, D.; Yuan, S.; Katsnelson, M.I.; Houston, J.; Smith, R.J.; McCloskey, D.; Donegan, J.F.; Coleman, J.N. Spectroscopic metrics allow in situ measurement of mean size and thickness of liquid-exfoliated few-layer graphene nanosheets. *Nanoscale* **2016**, *8*, 4311–4323. [CrossRef]
- 33. Nayak, L.; Rahaman, M.; Khastgir, D.; Chaki, T. Thermal and electrical properties of carbon nanotubes based polysulfone nanocomposites. *Polym. Bull.* **2011**, *67*, 1029–1044. [CrossRef]
- 34. Wang, Y.; Wang, L.; Yang, T.; Li, X.; Zang, X.; Zhu, M.; Wang, K.; Wu, D.; Zhu, H. Wearable and highly sensitive graphene strain sensors for human motion monitoring. *Adv. Funct. Mater.* **2014**, 24, 4666–4670. [CrossRef]
- 35. Moriche, R.; Sánchez, M.; Prolongo, S.G.; Jiménez-Suárez, A.; Ureña, A. Reversible phenomena and failure localization in self-monitoring GNP/epoxy nanocomposites. *Compos. Struct.* **2016**, 136, 101–105. [CrossRef]
- 36. Acquarelli, C.; Paliotta, L.; Tamburrano, A.; De Bellis, G.; Sarto, M.S. Electro-mechanical properties of multilayer graphene-based polymeric composite obtained through a capillary rise method. *Sensors* **2016**, *16*, 1780. [CrossRef]

Disclaimer/Publisher's Note: The statements, opinions and data contained in all publications are solely those of the individual author(s) and contributor(s) and not of MDPI and/or the editor(s). MDPI and/or the editor(s) disclaim responsibility for any injury to people or property resulting from any ideas, methods, instructions or products referred to in the content.